Ferroelectric response and induced biaxiality in the nematic phase of a bent-core mesogen

By O. Francescangeli[*], V. Stanic, S. I. Torgova, A. Strigazzi, N. Scaramuzza, C. Ferrero, I.P. Dolbnya, T. M. Weiss, R. Berardi, L. Muccioli, S. Orlandi, and C. Zannoni

[*] Prof. O. Francescangeli, Dr. V. Stanic
Dipartimento di Fisica e Ingegneria dei Materiali e del Territorio and CNISM
Università Politecnica delle Marche
Via Brecce Bianche I-60131 Ancona (Italy)
E-mail: o.francescangeli@univpm.it

Dr. S. I. Torgova
P.N. Lebedev Physical Institute of the Russian Academy of Sciences
Leninsky Pr. 53, Moscow, 119991 (Russia)

Prof. A. Strigazzi
Dipartimento di Fisica and CNISM
Politecnico di Torino
C.so Duca degli Abruzzi 24, I-10129 Torino (Italy)

Prof. N. Scaramuzza
LiCryl (CNR- INFM) and CEMIF.CAL, Dipartimento di Fisica
Università degli Studi della Calabria
Ponte P. Bucci C 31C, I-87036 Rende, Cosenza (Italy)

Dr. C. Ferrero, Dr. I. P. Dolbnya[+], Dr. T. M. Weiss[++]
European Synchrotron Radiation Facility
Boîte Postale 220, F-38043 Grenoble Cedex (France)

Dr. R. Berardi, Dr. L. Muccioli, Dr. S. Orlandi, and Prof. C. Zannoni
Dipartimento di Chimica Fisica e Inorganica and INSTM CRIMSON
Università di Bologna
Viale del Risorgimento 4, I-40136 Bologna, Italy

[+] Present address:
Diamond Light Source, Rutherford Appleton Laboratory
Chilton, Didcot, OX11 0QX (UK)
[++] Present address:
Stanford Synchrotron Radiation Laboratory
Menlo Park, CA 94025

[**] We thank EU–STREP Biaxial Nematic Devices (BIND) FP7-216025, INSTM and Fondazione CRT (FCRTnano project) for financial support. We are grateful to T. Narayanan, ESRF and W. Bras, Dubble CRG/ESRF, NWO for their support. We thank A. Pane, LiCryl, UNICAL, for the manufacturing of the cells and S. Marino, UNICAL, for co-work in the repolarization measurements. We are grateful to V. Torgov and B. Umanskii, Russian Acad. of Sciences, Moscow, for co-work in synthesis and conductivity characterization of the sample, respectively.

Supporting Information is available online from Wiley Interscience or from the authors.

Abstract

The still undiscovered fluid ferroelectric nematic phase is expected to exhibit a much faster and easier response to an external electric field compared to conventional ferroelectric smectic liquid crystals, therefore the discovery of such a phase could open new avenues in electro-optic device technology**.** We report the experimental evidence of a ferroelectric response to a switching electric field in a low molar mass nematic liquid crystal and argue its connection with field induced biaxiality. The fluid is made of bent-core polar molecules and is nematic over a range of 120 °C. Combining repolarization current measurements, electro-optical characterizations, x-ray diffraction and computer simulations we demonstrate the ferroelectric switching and conclude that the response is due to field-induced reorganization of polar cybotactic groups within the nematic phase. We believe that this represents a significant progress toward the realization of ferroelectric fluids that can be aligned at command with a simple electric field.

The search for the still undiscovered ferroelectric nematic (FN) liquid crystal (LC) phase is actively fuelled by the fascinating fundamental and technological perspectives offered by these materials, in particular due to their envisaged easy and fast response to an external electric field,[1,2] coupled to fluidity and self-healing ability typical of nematics that is crucial to their use in electro-optical devices.[3] The properties of this new phase of matter are expected to be very different from those of conventional ferroelectric liquid crystals (FLCs),[1, 4] which correspond to more solid-like smectic (Sm) phases, typically formed by chiral mesogens. The existence of FNLC is not forbidden from a theoretical point of view[5,6,7,8] and recent computer simulations have demonstrated polar fluid phases obtained from elongated asymmetric particles[9] with polyphilic character.[10] Unfortunately, despite years of intensive experimental quest, and claims that some achiral polymeric[11] and lyotropic[12] systems exhibit this phase, no successful demonstration of FNLCs has yet been given in low molecular weight thermotropic systems. Here we wish to report on a significant step in that direction and on the intriguing relation of this phase to the recently proposed induced biaxial nematic phase.[13]

A key requirement for a potential FN mesogen is its asymmetric shape, as that of bent-core mesogenic molecules (BM). Following the pioneering work of Niori et al.,[14] achiral BM have already been shown to yield a variety of Sm phases with ferro-, ferri- or antiferroelectric properties.[15,16,17] To display ferroelectric response in the nematic phase, molecules should organize so that their individual dipoles pile up coherently to produce a large overall polarization P_s, rather than canceling it out. BM seem promising in this respect, as their bow shape coupled with a transverse dipole could lead to a local packing favoring head-to-tail dipole arrangement and their consequent summing up. Although very few BM give fluid N phases, some of these present another much sought after liquid crystals feature, nematic biaxiality,[18,19,20,21] highlighting the rich possibilities offered by these new materials. Biaxiality and ferroelectricity appear to be strongly correlated. In particular Photinos et al.[13] have argued that the formation of a biaxial phase proceeds via the formation of locally biaxial clusters of BM that would be inevitably polar, thus greatly enhancing the electric susceptivity in the presence of a field.

Here we focus on a system composed of asymmetric 3,5-bis-{4-[4-(n-nonyloxy)benzoyloxy]phenyl}-1,2,4-oxadiazoles (9BPO),[22] presenting both tilted SmC and N phases[23,24] extending over a very wide temperature range (**Scheme 1**), for which

2. Results and Discussion

To investigate the nature of the phase organization and the extent of the related correlations we have first performed synchrotron X-ray diffraction (XRD) measurements on 9BPO at various temperatures. In particular we have studied the LC both in a glass capillary under a magnetic field ***B***, and as a thin film that can be aligned by an electric field ***E*** across a planar cell (**Figure 1A**). XRD data show the pattern for the nematic sample oriented with B=0.5 T at 150 °C (Figure 1B, 1C), similar to that observed by Acharya et al.[19] and Weissflog et al.[25,26] for BM with a symmetric oxadiazole core. The position of the wide angle crescents indicates that the BM align with their long molecular axis (***z*** in Scheme 1) parallel to the horizontal magnetic field ***B***.[27] The four symmetrically located diffuse spots in the small-angle X-ray scattering (SAXS) region hint at the presence of short–range SmC-like ordering (*cybotactic groups* or *clusters*)[28] in the N, a type of structure reported in the literature not only near a N-SmC transition but also over wide temperature ranges, even in the absence of an underlying SmC phase[29], and notably also for other BM.[30,26,31] At T=150 °C the center of SAXS peaks corresponds to a scattering vector ***q*** with modulus q_0=2.05 nm^{-1} and tilt β=49° from the ***B*** direction. The layer spacing in the cybotactic groups, $d=2\pi/q_0$=30.7 Å, is much smaller than the estimated molecular length (L_{MD}=35-50 Å depending on the chain conformation, with a maximum of the distribution function centered about 46.5 Å)[32] confirming a tilt comparable to β (inset of **Figure 2A**). Although for the symmetric oxadiazole compound in[19] the presence of cybotactic groups was ruled out and the SAXS pattern was interpreted in terms of the intrinsic BM structure,[33] in our case an analogous interpretation is not appropriate. In fact, in[19] the measured d-spacing corresponds to the estimated molecular length, whereas in our case the spacing compares well only after correction for the tilt angle, i.e. $d/\cos\beta \cong L$, clearly hinting to a tilted layered structure. This is further supported by the temperature dependence of the relevant structural parameters shown in Figure 2A, where d and β are seen to vary strongly over the nematic range yet maintaining the apparent molecular length $L=d/\cos\beta$ fairly constant and compatible with L_{MD}. Differently from,[19] we also find the longitudinal and transversal correlation lengths, calculated from the width of the SAXS peaks in the reciprocal space, to be strongly temperature dependent in the nematic range (see Figure 2B), a feature typical of cybotactic ordering.[28] Switching off the magnetic field, the four spots become wider diffuse arcs as the system slowly returns to an

about one hour at 157°C. On the contrary, a higher magnetic field increases significantly both longitudinal and transversal correlation lengths (filled symbols in Figure 2B).[34,13]

A second series of measurements has been carried out on thin films, using the setup sketched in Figure 1A (bottom). We have used planar cells of 20 μm thickness, which is much larger than the typical N or even Sm correlation lengths of up to ≈1 μm,[19] prepared using two conducting indium-tin oxide coated ultra-thin glass plates, covered with a film of evaporated SiO_x that causes strong and uniform alignment of the nematic director ***n*** along an in-plane direction ***r***.[35] The sample has a negative dielectric anisotropy, consistently with the large transverse dipole moment component ($\mu_x \approx 5$ D) of the BM, therefore surface anchoring and electric field (at any frequency) tend to orient the molecular ***z*** and ***x*** axes, respectively, parallel to their directions during the XRD measurements. With no applied field we have observed a SAXS four-spot pattern (Figure 1D) very similar to that obtained with the capillary samples aligned in the magnetic field (Figures 1B, 1C), confirming an effective alignment of ***z*** parallel to ***r***.[19] When ***E*** was applied, no changes were observed until the field strength exceeded a threshold value of about 7 V/μm, whereupon the four small angle reflections changed to an isotropic diffuse ring with the same radius (Figure 1E). The isotropy of the SAXS pattern under applied electric field is consistent with a field-induced reorientation of molecular dipoles (i.e. essentially of the short molecular axis ***x***) perpendicular to the glass slides, and with an isotropic distribution of the long axes around the field direction. The behavior we have observed is different from that reported in,[19] where the four small angle spots turn, above the field threshold, into two diffuse arcs centered on the equatorial line. On the contrary, our results are consistent with a model where polar cybotactic clusters, under applied field ***E***, reorient with their group dipole parallel to the field and the long molecular axes (hence the director ***n***) randomly distributed around ***E***. The bulk rotation of ***n*** consequent to such reorientation process has been confirmed by electro-optic measurements (c.f. Supporting Information, Videoclip 1).

To verify the presence of polar ordering we measured the electric response and switching behavior of 9BPO in the temperature range between T=120 °C and T=270 °C by means of the repolarization current technique[36] where an applied triangular voltage waveform drives a current through a thin film of material, measured by the voltage drop across a high precision resistor connected in series with the sample (capacitor) and the voltage generator.

Consistently with the X-ray experiment with an applied electric field, above a threshold

from the reversal of the polarization direction in the LC sample gives a nonlinear contribution to the total current superimposed to the linear background generated by the ionic flow,[36,37] as shown in **Figure 3A**. The observed ferroelectric response indicates, differently from normal nematics, the existence of a switchable macroscopic bulk polarization in the direction of the applied electric field, and hence of polar ordering. The single peak shown by the current profile within each half-period after the voltage sign change (*delayed* peak) indicates that the polarization vector rotates without vanishing, thus implying a ferroelectric ordering[36] both in the Sm and N mesophases. We observed a similar behavior over the entire nematic range up to the clearing temperature, while in the isotropic phase the peak completely disappears (inset of Figure 3A), thereby excluding spurious contributions such as sample impurities or surface effects. Further evidence of this polar switching is provided by the electro-optic response of the sample observed with a polarized optical microscope (see Supporting Information, Videoclips 2-3). This electric response is different from that expected for paraelectric phases (even what could be called *super*- or *nonlinear*-paraelectric, given the high P_s values involved) that do not show any switching threshold and whose polarization switching should exhibit a single peak per half-period centered at the zero-crossing point of the applied voltage.[36]

The unique delayed peak per half-period observed in the repolarization measurements under triangular wavevoltage shows[36,38] that the polarization vector $\boldsymbol{P}_s$ (whose characteristic lifetime is greater than the half-period of the input voltage) rotates at constant modulus. The electric response is therefore the same observed in *true* ferroelectrics, i.e. ferroelectric materials having an ideally infinite lifetime of the polarization, even if our field-on ferroelectric nematic phase eventually goes back to a non polar ground phase as the field is definitively switched off. Although there is no universally accepted definition of ferroelectrics, as pointed out in the classical work of Lines and Glass,[39] this behavior is consistent with that of ferroelectrets.[39] To rule out the possibility that the recorded peaked polarization response is generated by a field-induced N-SmC phase transition, particularly in view of the low temperature SmC phase of the material, we extended the XRD study so as to characterize the structure of the sample in the switched state, i.e. the state after the appearance of repolarization current peak in Figure 3A. The measurements were carried out by subjecting the cell sample to a low frequency square-wave voltage (ν=0.1 Hz, duty cycle=50%) with amplitude above threshold, and taking XRD spectra before and after the voltage step rise

4, where A and B refer to *before* and *after* the step rise, respectively. These measurements provide clear evidences of the *nematic* nature of the sample before and after the switching current peak. In fact, the broad diffuse ring in B is the signature of a N phase isotropically oriented around the incident beam. The change of the pattern from the *normal* state (A) to the *switched* state (B) is the same observed in Figure 1D-E and is consistent with the persistence of the cybotactic N in which the electric field simply induces a reorientation of the polar domains. The dynamics of the cluster reorientation has been investigated by means of time-resolved XRD measurements. Using the same planar cell, we have studied the relaxation from the *polar* to the *non-polar* N phase after the dc electric field above threshold is switched off. XRD spectra were taken at regular intervals of 0.5 s, with an acquisition time of 0.5 s (i.e. the minimum accessible with the present setup because of the low scattering of the thin cell). The orientation relaxation is monitored following the evolution of the pattern from the initial isotropic diffuse ring into the final anisotropic four-spots pattern. The results in Figure 4C-F clearly show that the time-scale of the relaxation process (i.e. the time for the cybotactic clusters to rotate back to the initial non-polar configuration) is of the order of the second.

The macroscopic bulk, field on, polarization P_s has been obtained experimentally integrating the switching current over one half-period after subtracting the linear background, and dividing by twice the electrode area.[37] Figure 3B (blue squares) shows P_s as a function of the temperature. We see that P_s increases with temperature up to 190°C, well inside the nematic range, where it reaches a maximum value of about 100 nC/cm^2. The value of P_s is quite significant and of the same order of magnitude as that obtained for typical SmC* FLCs reported in literature (now values of a few hundred nC/cm^2 are available, but the first one was $P_s \approx 5$ nC/cm^2,[4] while for the first BM FLC it was $P_s \approx 50$ nC/cm^2 [14]). Rather surprising is, instead, the initial rise in P_s with temperature, opposite to the usual decrease. [40,41,38] In addition, no appreciable discontinuity of P_s at the SmC-N phase transition is observed even though a slight change of the slope of the polarization curve may be captured across the phase boundary.

In order to understand the molecular mechanisms underlying the onset of polarization, we have performed a detailed modeling and simulation of the structure of the system: we have employed Density Functional Theory (DFT)[42] calculations to determine the 9BPO geometry and charge distribution, then we have run atomistic molecular dynamics (MD) simulations, including the DFT charges in the force field, to obtain a realistic distribution of conformations, and the local structure of the LC around each mesogen.[43,44] Hence we have

Berne,[45,46] dipolar ellipsoids[47] (see Scheme 1 and Tables 1-2), whose optimized dimensions, positions and orientations have been derived from the MD trajectories by an analysis of the centers of mass and gyration radii, while the three point dipoles were derived by fitting the DFT dipoles calculated for the aromatic core in a planar geometry, averaging the possible orientations of the carbonyl bonds. Starting from this model, we have performed constant pressure Monte Carlo (MC) simulations at different temperatures with 1000 BMs and periodic boundaries. We found I, N and SmC phases with T_{NI}≈265 °C and $T_{SmC.N}$≈140 °C in good agreement with the experiments, obtaining a first validation of the model. Analyzing the quadrupolar and polar radial pair correlations $S_{22}^{220}(r)$ [48] and $P_{1x}(r)$ (defined in the Supporting Information), we have found that the N phase contains indeed cybotactic groups, with *local* polar and biaxial ordering in the direction of the ***x*** molecular axis. Their average size ξ, obtained from the decay of these correlation functions, decreases with temperature from ξ≈30 Å at 150 °C to ξ≈16 Å at 260 °C, in qualitative accord with the XRD results. In[47] a similar model, but devoid of the central dipole, was shown to form N and SmA phases but not cybotactic clusters, while a model with one central **x** dipole gave only a SmB phase. A comparison with the simulations results[20] for the symmetric oxadiazole in[18,19] highlights numerous similarities and suggests attributing to the asymmetry of the central dipole a significant increase of the nematic range.

As expected, the simulated system does not show overall spontaneous polarization $\boldsymbol{P}_s = \left\langle \sum_{i=1}^{N} \boldsymbol{\mu}_i / V \right\rangle$; however, to compare with repolarization measurements, an electric field must be applied also to the MC sample. We have therefore studied the changes of molecular organization and of $\boldsymbol{P}_s$ in the presence of a static electric field ***E*** perpendicular to ***n***, adding to the potential energy a linear and a quadratic (dielectric) term in which ***E*** is coupled with the molecular dipoles.[48] We have found that, while the uniaxial order parameter R_{00}^2 [49] remains relatively unaffected by the field, when ***E*** is on, the system exhibits a large induced polarization increasing and then decreasing with temperature, as shown in Figure 3B (red squares), in excellent agreement with the repolarization current measurements (blue squares).[50]

Due to the particular shape of 9BPO, macroscopic polarization is expected to be coupled to biaxiality.[51,13] While the latter is hard to be unambiguously measured experimentally,[18,19,52,53] and could not be determined in this work, it can be directly

that the application of the electric field ***E*** determines a considerable increase of R_{22}^2 (shown in Figure 3B as $\Delta R_{22}^2 = R_{22}^{2\,(\boldsymbol{E})} - R_{22}^{2\,(0)}$). In practice, the simulations of a nematic monodomain show that the field induces a reorganization from a uniaxial N with cybotactic groups to a biaxial polar N, in agreement with the theory of Vanakaras and Photinos.[13]

From Figure 3B it is also clear that the temperature behavior of this field-induced biaxiality is closely related to that of $\boldsymbol{P}_s$. When ***E*** is switched off instead, the two types of correlation are lost with different decay times: while polarization vanishes at all temperatures in a few MC kcycles, biaxiality is retained for long times if T<190 °C, i. e. at temperatures below the polarization peak. To confirm the molecular origin of the switching and its relation to phase biaxiality we have performed a simulation in the presence of a square wave field (Figure 3C) at T=190 °C. The results show: i) the reorientation of the clusters when the sign of the applied electric field reverses during the run (see the alternate prevalence of red and blue domains in the different snapshots); ii) the linearity of the coupling between $\boldsymbol{P}_s$ and ***E*,** i.e. the sign of polarization (blue squares) follows the sign of the applied field (red line); iii) the induction of biaxiality[57], almost insensitive to the change of sign of the field, and its disappearance when the field is switched off.

On the basis of these findings, we suggest two possible explanations of the temperature behaviour of polarization. In the first, the dimensions of the polar cybotatic clusters (the building blocks for macroscopic electric susceptibility) decreases with T while the field-induced reorientation of the clusters becomes easier at increasing T because of the reduced viscosity. The competition between these two phenomena determines the unusual behavior of P_s. In the second, which does not exclude the first, and is inspired by the phase diagrams in[13], we suppose that at T≈190 °C a phase transition takes place for the induced biaxial phase, which is stable (or metastable) at T<190 °C and becomes unstable at T>190 °C. Further experiments are needed to verify these hypotheses, but in any case the role of viscosity is manifested by the frequency dependence of the threshold field measured in both repolarization and XRD experiments. In fact the threshold voltage for the onset of polarization switch was found to increase on increasing frequency, up to the maximum value experimentally accessible (V_{pp}=500 V at v=50 Hz). In a similar way, the threshold field for the onset of the switched state probed by XRD was observed to increase continuously over the whole explored frequency range (0.1 Hz - 5 KHz).

On the basis of the experimental and simulation results the switching mechanism of the 9BPO can be pictured as follows. The nematic phase consists of a conglomerate of nano-sized cybotactic groups featuring short-range SmC-like ordering. Each group exhibits local biaxial and polar (i.e. ferroelectric) ordering due to the cooperative alignment of the molecules with their short axes and electric dipoles parallel to each other. In the absence of an electric field $\boldsymbol{E}$, the orientations of the domains are randomly distributed in space and, as a result, the macroscopic polarization $\boldsymbol{P_s}$ averages to zero. Applying $\boldsymbol{E}$ above a certain threshold converts this non-polar phase into a polar nematic in which the cybotactic groups are on the average aligned with their dipoles parallel to the applied field over macroscopic volumes. A net bulk polarization is then induced and its direction can be reversed by changing the sign of $\boldsymbol{E}$. Once the polar state has settled, this switching can simply take place through the cooperative rotation of the BM of each group about the long molecular axis (with the local biaxial order persisting during field reversal) and does not necessarily involve further rotation of the clusters. In fact, as pointed out by the time-resolved XRD measurements, the cluster reorientation is too slow to be compatible with the switching response that we could measure up to frequencies of several tens of Hz. In the SmC phase the switching mechanism of the 9BPO should be very similar. Here, application of an electric field **E** above threshold reorients the smectic microdomains with the polar axes (hence the smectic planes) parallel to $\boldsymbol{E}$ and the normal to the smectic layers randomly distributed about $\boldsymbol{E}$. This is shown by the XRD data collected at T=130°C in the SmC phase (see **Figure 5**). Once this polar state is settled, the polarization reversal upon change of the $\boldsymbol{E}$ sign still can occur simply involving the cooperative rotation of the BM around the long axis. Because this mechanism does not need a *domain* rotation, it can take place while the SmC-layer structure is being preserved. The similarity of the switching is the N and SmC phase is confirmed by the electro-optical measurements carried out at T=130°C in the SmC phase (see Supporting Information, Videoclip 4). We believe that the continuity of the polarization P_s across the N-SmC transition can be explained by this analogy of the switching mechanism in the two phases.

In conclusion, we have shown evidence of a ferroelectric response in a low molar mass nematic material and argued its connection with field induced biaxiality. We believe that this represents a significant progress toward the realization of ferroelectric fluids that can be aligned at command with a simple electric field.

4. Experimental

X-ray diffraction: The X-ray diffraction (XRD) measurements on samples in sealed glass capillaries (2 mm diameter) were carried out at the Dutch-Flemish beamline (BM26 "DUBBLE") of the European Synchrotron Radiation Facility (ESRF) in Grenoble (France), using a 15 KeV X-ray beam (λ= 0.827 Å, spot size 0.3×0.3 mm^2). The diffracted intensity was collected at 1.5 m distance on a two-dimensional gas-filled detector (512×512 pixels). XRD spectra in the wide angle region were obtained by reducing the sample-to-detector distance to 0.5 m and using a 18 KeV X-ray beam (λ = 0.690 Å). The capillaries were standing orthogonal to the incident X-ray beam. The temperature of the sample was controlled with an accuracy of ±0.1 ˚C. The experimental setup allowed the application of a magnetic field of variable intensity (up to 1 T) perpendicular to the plane defined by the capillary and the X-ray beam.

The small angle XRD measurements were carried out on thin planar sample cells at the SAXS beamline ID02 of the ESRF. The energy of the incident beam was 12.5 KeV (λ = 0.995 Å), the beam size was 0.1×0.1 mm^2, and the sample-to-detector distance was 1.5 m. The diffraction patterns were collected on a two-dimensional CCD detector (1024×1024 pixels). Cells of 20 μm thickness were prepared using two thin glass plates coated with a conductive ITO-film (50 μm thick). The glass plates were further coated with a thin SiO_x film deposited under vacuum at an evaporation angle of 60° in order to achieve strong planar anchoring of the molecules and homogeneous in plates orientation of the nematic director ***n***. The cells were then assembled with the glass plates facing their coated sides in a parallel-plane configuration and separated by high precision spacers. Finally, the cell (1cm x 1cm) was filled by capillarity, the LC being in the fluid phase and then slowly cooled down to room temperature and then mounted on a special temperature-controlled hot stage allowing the insertion of a static magnetic field (of variable intensity up to 1 T) perpendicular to the incident X-ray beam. This cell was used to apply a low frequency (0-1 KHz) electric field ***E*****,** parallel to the X-ray beam, across the conductive plates (see Figure 3).

Electric Polarization: The measurements employed a 10-μm-thick sandwich-cell with the LC confined between two conducting indium tin oxide (ITO)-coated glass plates covered with an aligning layer of vacuum deposited SiO_x. The cell was initially filled up with the LC in the N phase (at T=200˚C) and cooled down at a rate of -0.1˚C/min to the crystalline phase at room

hot stage, remotely driven by a PC, which can reach 350 ˚C with temperature stability better than 0.1˚C.

Modeling and simulation: Atomistic MD simulations of a sample of N=150 united-atoms (UA) 9BPO molecules were run in the NpT ensemble at atmospheric pressure and at the following temperatures: 127, 152, 177, 202, 227, 252, 277, 302, 327 °C. We used the NERD UA force field [58] for alkyl chains and the AMBER UA force field [59] completed with B3LYP//6-31G* ESP atomic charges [60] for the aromatic core of the molecules. The runs were performed with the multiple time step code ORAC [61], using a maximum time step of 10 fs, 3D periodic boundary conditions, and the SPME method [62] for calculating long range electrostatic interactions.

Starting from a box with molecules placed on a cubic lattice, the sample was progressively heated with equilibration runs of at least 20 ns, followed by production runs of at least 10 ns. The system was found to be still nematic at T=277 °C, but it became isotropic in the subsequent simulation at T=302 °C, thus showing that isotropization occurs between 277 °C and 302 °C in reasonable agreement with the experimental T_{NI} value of 263 °C.

The trajectory at 225 °C was used for deriving the shape parameters of the coarse grained model constituted by three elongated ellipsoids: this was accomplished by virtually dividing 9OCD into three fragments (2 x (alkyl chain+phenyl), 1 x COO-Ph-oxa-Ph-COO) and calculating the average center of mass and gyration radius components of each of them. A bending angle (i.e. the opening angle between the two lateral rods) of 120° was found, while the final dimensions of the ellipsoids (in Table 1) were obtained adding to the components the value of 3.4 Å (van der Waals diameter for carbon) and 2 Å along the interconnection direction (z) to allow for a good superposition between connected sites. The centers of mass were shifted to account for this superposition. The values and the orientation of the three point dipoles were calculated by a least square fit of the DFT total dipole calculated for the aromatic core in all the different planar geometries with carbonyl groups pointing "up" or "down", while their positions match the centers of the oxadiazole ring and of the COO groups.

Table 1. Dimensions σ_x , σ_y , σ_z and positions r_x , r_y , r_z (in σ_0 units), potential well depths ε_x , ε_y , ε_z (in ε_0 units) of the three GB sites constituting the molecular model.

GB Site	σ_x	σ_y	σ_z	r_x	r_y	r_z	ε_x	ε_y	ε_z
1	0.7	5.5	2.4	0	0	0	1.0	1.4	0.5

2	0.6	0.5	1.2	0.21	0	+1.36	0.8	0.8	0.25
3	0.6	0.5	1.2	0.21	0	-1.36	0.8	0.8	0.25

Table 2. Components μ_x, μ_y, μ_z (D) and positions r_x , r_y , r_z (in σ_0 units) of the three point dipoles.

Dipole site	μ_x	μ_y	μ_z	r_x	r_y	r_z
1	3.9	0	-1.9	-0.11	0	0
2	1.7	0	-2.3	0.10	0	+0.68
3	1.7	0	+2.3	0.10	0	-0.68

MC simulations of 1000 coarse-grained three-sites GB [45] dipolar BM were performed in the isobaric-isothermal *NpT* ensemble with periodic boundary conditions at p^*=8 and in the temperature range T^*=2.8-4.8, which, assuming a scaling factor $\varepsilon_0=kT_{NI}/T_{NI}^*=150\times10^{-23}$ J and $\sigma_0=10^{-9}$ m, corresponds to T=120-300 °C and p=12 MPa. Simulations started from an equilibrated configuration in the isotropic phase (T=300 °C) and were carried out in a cooling sequence of runs down to T=110 °C, starting from the final equilibrated configuration obtained at the upper temperature. The equilibration length varied from 400 kcycles up to 800 kcycles. A variable metric tensor was used in order to allow shape changes of the MC box to take place[47]. Dipole-dipole interactions were evaluated using the reaction field method.

In a second set of simulations, field-on experiments were performed adding a field-dipole coupling term [48] to the three-site GB potential. The field contribution for each dipole in the molecule is considered as the first two anisotropic terms of a general expansion of the interaction energy in power of the field strength:

$$U_i = -k_1\mu_i\,(\hat{\boldsymbol{\mu}}_i \cdot \hat{\boldsymbol{E}}) - k_2\mu_i^2 \left[\frac{3}{2}(\hat{\boldsymbol{\mu}}_i \cdot \hat{\boldsymbol{E}})^2 - \frac{1}{2}\right]$$

with the coupling parameters k_1=1, k_2=0.5 were chosen to get the same order of magnitude for the first and second rank energetic terms and a global field energy contribution around 25 % of the total potential energy in the SmC and N phases. After applying the field perpendicularly to the phase director, the BM were found to align their transverse dipoles

polarization.

Received: ((will be filled in by the editorial staff))
Revised: ((will be filled in by the editorial staff))
Published online: ((will be filled in by the editorial staff))

[1] J. W. Goodby, R. Blinc, N.A. Clar, S. T. Lagerwall, M. A. Osipov, S. A. Piking, T. Sakurai, K. Yoshino, B. Zeks, in *Ferroelectric Liquid Crystals*, Gordon and Breach, Philadelphia, USA **1991**.

[2] L. M. Blinov, *Liq. Cryst.* **1998**, *24*,143-152.

[3] S. T. Lagerwall, in *Handbook of Liquid Crystals Vol. 2B*, (Eds.: D. Demus), Wiley-VCH, Weinheim, DE **1998**.

[4] R.B. Meyer, L. Liébert, L. Strzelecki, P. Keller, *J. Phys.* (Paris) **1975**, *36*, 69-71.

[5] D. Wei, G. N. Patey, *Phys. Rev. Lett.* **1992**, *68*, 2043-2047.

[6] J. J. Weis, D. Levesque, G. J. Zarragoicoechea, *Phys. Rev. Lett.* **1992**, *69*, 913-916.

[7] P**.** Palffy-Muhoray**,** M. A**,** Lee, R. G. Petschek, *Phys. Rev. Lett.* **1998**, *60*, 2303-2306.

[8] B. Park, J. W. Wu and H. Takezoe, *Phys. Rev. E* **2001**, *63*, 021707.

[9] R. Berardi, M. Ricci, C. Zannoni, *ChemPhysChem* **2001**, *2*,443-447.

[10] F. Tournilhac, L. M. Blinov, J. Simon, S. V. Yablonsky, *Nature* **1992**, *359*, 621-623.

[11] T. Watanabe, S. Miyata, T. Furukawa, H. Takezoe, T. Nishi, M. Sone, A. Migita, J. Watanabe*, Jpn. J. Appl. Phys.* **1996**, *35*, 505-507.

[12] C.-C. Yen, Y. Taguchi, M. Tokita and J. Watanabe, *Macromolecules* **2008**, *41*, 2755-2758.

[13] A. G. Vanakaras, D. J. Photinos, *J. Chem. Phys*. **2008**, *15*, 154512.

*6***,**1231-1233.

[15] G. Pelzl, S. Diele, W. Weissflog, *Adv. Mater***. 1999**, *11*, 707-724.

[16] D. R. Link, G. Natale, R. Shao, J. E. Maclennan, N. A. Clark, E. Korblova, D. M. Walba, *Science* **1997**, *278*, 1924-1927.

[17] D. A. Coleman, J. Fernsler, N. Chattham, M. Nakata, Y. Takanishi, E. Korblova, D. R. Link, R. F. Shao, W. G. Jang, J. E. Maclennan, O. Mondainn-Monval, C. Boyer, W. Weissflog, G. Pelzl, L. C. Chien, J. Zasadzinski, J. Watanabe, D. M. Walba, H. Takezoe, N. A. Clark, *Science* **2003,** *301*, 1204-1211.

[18] L. A. Madsen, T. J. Dingemans, M. Nakata, E.T. Samulski, *Phys. Rev. Lett.* **2004,** *92*, 145505.

[19] B. R. Acharya, A. Primak, S. Kumar, *Phys. Rev. Lett.* **2004,** *92*, 145506.

[20] J. Peláez, M. R. Wilson, *Phys. Rev. Lett.* **2006**, *97*, 267801.

[21] R. Berardi, L. Muccioli, S. Orlandi, M. Ricci, C. Zannoni, *J. Phys***.***: Condens. Matter* **2008**, *20*, 463101.

[22] S. I. Torgova, L. A. Karamysheva, T. A. Geivandova, A. Strigazzi, *Mol. Cryst. Liq. Cryst.* **2001**, *365*, 1055-1062.

[23] S. I. Torgova, T. A. Geivandova, O. Francescangeli, A. Strigazzi, *Pramana* **2003**, *61*, 239-248.

[24] In ref. [23], based solely on preliminary x-ray diffraction measurements on unoriented powder, the smectic phase of 9BPO was assigned SmA instead of SmC.

[25] W. Weissflog, S. Sokolowski, H. Dehne, B. Das, S. Grande, M. W. Schroder, A. Eremin, S. Diele, G. Pelzl, H. Kresse, *Liq. Cryst.* **2004**, *31*, 923-933.

[26] H. Takezoe and Y. Takanishi, *Jpn. J. Appl. Phys.* **2006**, *45*, 597-625.

Chemical Properties and Methods of Investigation, (Eds.: G. W. Gray, P. Winsor), Ellis Horwood, Chichester, UK **1974**, pp. 62-79.

[28] A. De Vries A, *Mol. Cryst. Liq. Cryst.* **1970**, *10*, 219-236.

[29] O. Francescangeli, M. Laus, G. Galli, *Phys. Rev. E* **1997**, *55*, 481-487.

[30] S. Stojadinovic, A. Adorjan, S. Sprunt, H. Sawade, A. Jakli, *Phys. Rev. E* **2002**, *66*, 060701.

[31] E. Cavero, D. P. Lydon, S. Uriel, M. R. de la Fuente, J. L. Serrano, R. Giménez, *Angew. Chem. Int. Ed.* **2007**, *46*, 5175-5177.

[32] As in [43, 44], the effective molecular length L_{MD} is estimated from the distribution of the largest dimension of the minimum volume box containing the molecule rotated in its inertial frame, obtained from the atomistic MD simulation at 227 °C described in the experimental and supporting information sections.

[33] B. R. Acharya, S. W. Kang, S. Kumar, *Liq. Cryst.* **2008**, *35*, 109.

[34] V. Domenici V, C. A. Veracini CA, K. Fodor-Csorba, G. Prampolini, I. Cacelli I, A. Lebar, B. Zalar, *ChemPhysChem*, **2007**, *8*, 2321-2330.

[35]. M. Monkade, P. Martinot-Lagarde, G. Durand, C. Granjean, *J. Phys. II* **1997**, *7*, 1577-1596.

[36] M. F. Achard, J. P. Bedel, J. P. Marcerou, H. T. Nguyen, J. C. Rouillon, *Eur. Phys. J. E* **2003**, *10*, 129-134.

[37] K. Miyasato, S. Abe, H. Takezoe, A. Fukuda, E. Kuze, *Jap. J. Appl. Phys. Lett.* **1983**, *22*, 661-663.

[38] K. Nishida, M. Cepic, W. J. Kim, S. K. Lee, S. Heo, J. G. Lee, Y. Takanishi, K. Ishikawa, K.-T. Kang, J. Watanabe, H. Takezoe, *Phys. Rev. E* **2006,** *74*, 021704.

[39] M. Lines and A. Glass, in *Principles and Applications of Ferroelectrics and Related Materials*, Oxford U.P., Oxford, UK **2001**, pp. 546.

[41] H. Nádasi, W. Weissflog, A. Eremin, G. Pelzl, S. Diele, B. Das and S. Grande, J. *Mater. Chem.* **2002**, *12*, 1316-1324.

[42] W. Koch W, M. Holthausen, in *A Chemist's Guide to Density Functional Theory*, Wiley-VCH Verlag, Weinheim, DE **2001**.

[43] R. Berardi, L. Muccioli, C. Zannoni, *ChemPhysChem* **2004**, *5*, 104-111.

[44] G. Tiberio, L. Muccioli, R. Berardi, C. Zannoni, *ChemPhysChem* **2009**, *10*, 125-136.

[45] J.G. Gay and B.J. Berne, *J. Chem. Phys.* **1981**, *74*, 3316-3319.

[46] C. Zannoni, *J. Mater. Chem.* **2001**, *11*, 2637-2646.

[47] S. Orlandi, R. Berardi, J. Stelzer, C. Zannoni, *J. Chem. Phys.* **2006**, *124*, 124907.

[48] R. Berardi, S. Orlandi, C. Zannoni, *PCCP* **2000**, *2*, 2933-2942.

[49] C. Zannoni, in *Advances in the Computer Simulations of Liquid Crystals*, (Eds.: P. Pasini, C. Zannoni), Kluwer, Dordrecht, NL **2000**, pp. 17-50.

[50] To compare the experimental and theoretical polarization values, a scaling factor was required and thus we have scaled the value at 190 °C in Figure 3B to the experimental one, but otherwise no fitting has been performed.

[51] H. R. Brand, P. E. Cladis, H. Pleiner *Int. J. Eng. Science* **2000**, *38*, 1099-1112.

[52] C. Cruz, J. L. Figueirinhas, D. Filip, G. Feio, A. C. Ribeiro, Y. Frère, T. Meyer, G. H. Mehl, *Phys. Rev. E* **2008**, *78*, 051702; C. D. Southern, P. D. Brimicombe, S. D. Siemianowski, S. Jaradat, N. Roberts, V. Görtz, J. W. Goodby, H. F. Gleeson, *Europhys. Lett.* **2008**, *82*, 56001.

[53] G. R. Luckhurst, *Nature* **2004**, *430*, 413-414.

[54] F. Biscarini, C. Chiccoli, P. Pasini, F. Semeria, C. Zannoni, *Phys. Rev. Lett.* **1995**, *75*, 1803-1806.

[55] R. Berardi, C. Zannoni, *J. Chem. Phys.* **2000**, *113*, 5971-5979.

[57] D. A. Dunmur, K. Szumilin, T. F. Waterworth, *Mol. Cryst. Liq. Cryst.* **1987**, 149, 385-392.

[58] S. K. Nath, F. A. Escobedo, J. J. de Pablo, *J. Chem. Phys.* **1998**, *23*, 9905-9911.

[59] W. D. Cornell, P. Cieplak, C. I. Bayly, I. R. Gould, K. M. Merz, D. M. Ferguson, D. C. Spellmeyer, T. Fox, J. W. Caldwell, P. A. Kollman, *J. Am. Chem. Soc.* **1995**, *117*, 5179-5197.

[60] J. M. Wang, R. M. Wolf, J. W. Caldwell, P. A. Kollman, D. A. Case, *J. Comput. Chem.* **2004**, *25*, 1157-1174.

[61] P. Procacci, T. A. Darden, E. Paci, M. Marchi, *J. Comput. Chem.* **1997**, *18*, 1848-1862.

[62] T. Darden, D. York, L. Pedersen, *J. Chem. Phys.* **1993**, *98*, 10089-10092.

Scheme 1.

Top: the phase sequence and transition temperatures of the 9BPO bent-core mesogen as measured by both heating and cooling differential scanning calorimetry experiments [23].

Middle: Chemical structure of 9PBO.

Bottom: scheme of the Gay-Berne dipolar model employed in the Monte Carlo simulations, showing the three sites as blue ellipsoids and the electric dipoles as red arrows.

Figure 1.

(A) Schematic drawing of the experimental XRD setups (left) and synchrotron XRD patterns from the N phase at T=150 °C (right) with the thin film sample aligned by a magnetic (*B*) or electric (*E*) field applied either perpendicular to the beam direction or parallel to it.

The four images refer to (B) a capillary sample with B=0.5 T; (C) a close-up of the small angle region in image (B) showing the four symmetrically located diffuse spots as obtained at the BM26 beamline, ESRF; (D) a thin (20 μm) LC film sandwiched between SiO_x-covered glass plates aligning the director $\boldsymbol{n}$ in the LC cell parallel to $\boldsymbol{r}$ with B=0, E=0, and (E) the same cell with B=0 and E= 7.5 V/μm, 500 Hz, as obtained at the ID02 beamline, ESRF. In all patterns, the magnetic field lies along the horizontal axis.

Figure 2.

(A) Structural parameters relevant to the cybotactic ordering as a function of temperature: d is the layer spacing, β is the tilt angle and $L=d/\cos\beta$ is the apparent molecular length. In the inset, a simulation snapshot showing a few cybotactic groups with a representation of the above physical quantities.

(B) Spatial longitudinal ($\xi_{\parallel}$, blue squares) and transversal ($\xi_{\perp}$, red circles) correlation length, as a function of temperature, for two magnetic field values: 0.5 T (empty symbols) and 1.0 T (filled symbols). These quantities are calculated as $\xi_{\parallel,\perp}=2/\Delta q_{\parallel,\perp}$, where $\Delta q_{\parallel}$ and $\Delta q_{\perp}$ are the full width at half maximum (FWHM) of the Lorentzian lineshapes describing the profiles of the small-angle peaks in the reciprocal space, parallel and orthogonal to the magnetic field direction, respectively.

(C) Synchrotron SAXS patterns as a function of temperature. From the left to the right T=150, 170, 200, 220, 245 and 270 ˚C. Color coding (blue-green-yellow-purple red) for XRD

The magnetic field lies along the horizontal axis, as shown in Fig. 1A.

Figure 3.
(A) Switching current response for 10 μm cell thickness, measured at T=120 °C (Sm, blue squares), 150 °C (N, red dots), 265 °C (I, in the inset, green), upon applying a triangular wave voltage (ν=1.1 Hz, V_{pp}=200 V, violet continuous line).
(B) Transverse polarization P_s response to an electric field E, as a function of the temperature, both from experiments (blue squares) and from MC simulations (red squares). The error bars are calculated from the statistical treatment of the repolarization current data over several periods of the input wave voltage. The difference between field-off and field-on biaxiality $\Delta R_{22}^2 = R_{22}^{2\,(\boldsymbol{E})} - R_{22}^{2\,(0)}$ (cyano circles) vs T is also reported.
(C) MC evolution, at T=190 °C, in the presence of an electric field $\boldsymbol{E}$ switching its sign every 250 kcycles and turned off after 900 kcycles. The instantaneous transversal (e.g. normal to the director) polarization P_{sx} (blue line, scale on the left) follows the field profile (cyan dashed line) with a delay of about 100 kcycles. The biaxiality order parameter R_{22}^2 (red line, scale on the right) grows almost irrespective of the field sign. The snapshots of the system after 250, 500, 750 and 1150 kcycles, show the alternation of prevalently red and blue polar domains depending on the sign of $\boldsymbol{E}$, and the eventual recovering of a non ferroelectric, uniaxial state.

Figure 4.
(A)-(B) Synchrotron XRD patterns from a thin (20 μm) sample film subjected to a low frequency square-wave voltage (ν=0.1 Hz, duty cycle=50%) above threshold: (A) before and (B) after the voltage step rise corresponding to the onset of the switching repolarization current peak. The film is sandwiched between SiO_x-coated glass plates aligning the director $\boldsymbol{n}$ in the LC cell parallel to $\boldsymbol{r}$. The temperature is T=150°C and the magnetic field is zero.
(C)-(F) Time resolved synchrotron XRD patterns of the same cell sample at T=150°C in the N phase: (C) dc E-field on (above threshold), and (D) 1 s, (E) 2 s, (F) 10 s and after switching off the field. The acquisition time per frame is 0.5 s. No magnetic field is applied.

Figure 5.
Small-angle XRD diffraction patterns of the planar thin-film cell sample at T=130°C in the SmC phase. (A) SmC uniaxially oriented by the planar surface anchoring parallel to the horizontal axis $\boldsymbol{r}$, when $\boldsymbol{E}$=0 and $\boldsymbol{B}$=0. (B) SmC after application of an electric field $\boldsymbol{E}$ above

with a reorientation of the smectic domains with the polar axes parallel to the ***E*** and the normal to the smectic layers randomly distributed about ***E***. (C) SmC under the same ***E*** field in the presence of a magnetic field ***B***=1.1 T parallel to ***r***. A comparison with pattern A shows that no domain reorientation takes place when a magnetic field of enough strength is applied parallel to ***r*** to fix the long molecular axis.

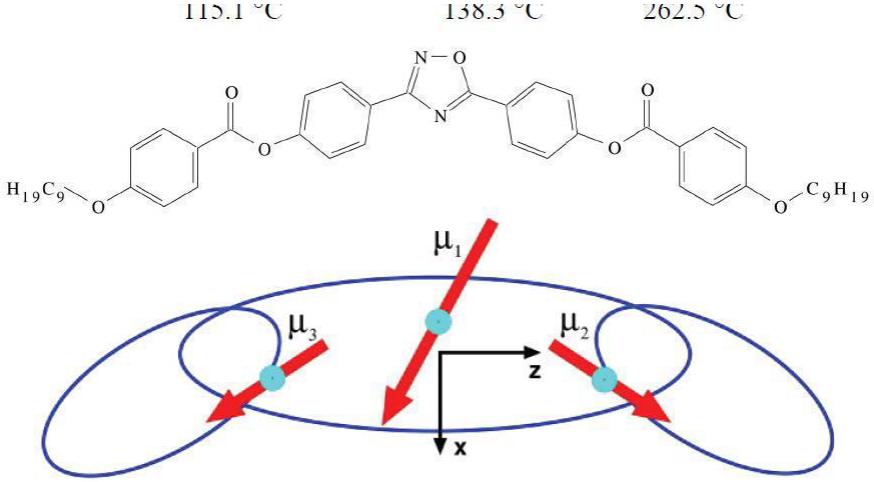

Scheme 1.

Top: the phase sequence and transition temperatures of the 9BPO bent-core mesogen as measured by both heating and cooling differential scanning calorimetry experiments [23]

Middle: Chemical structure of 9PBO.

Bottom: scheme of the Gay-Berne dipolar model employed in the Monte Carlo simulations, showing the three sites as blue ellipsoids and the electric dipoles as red arrows.

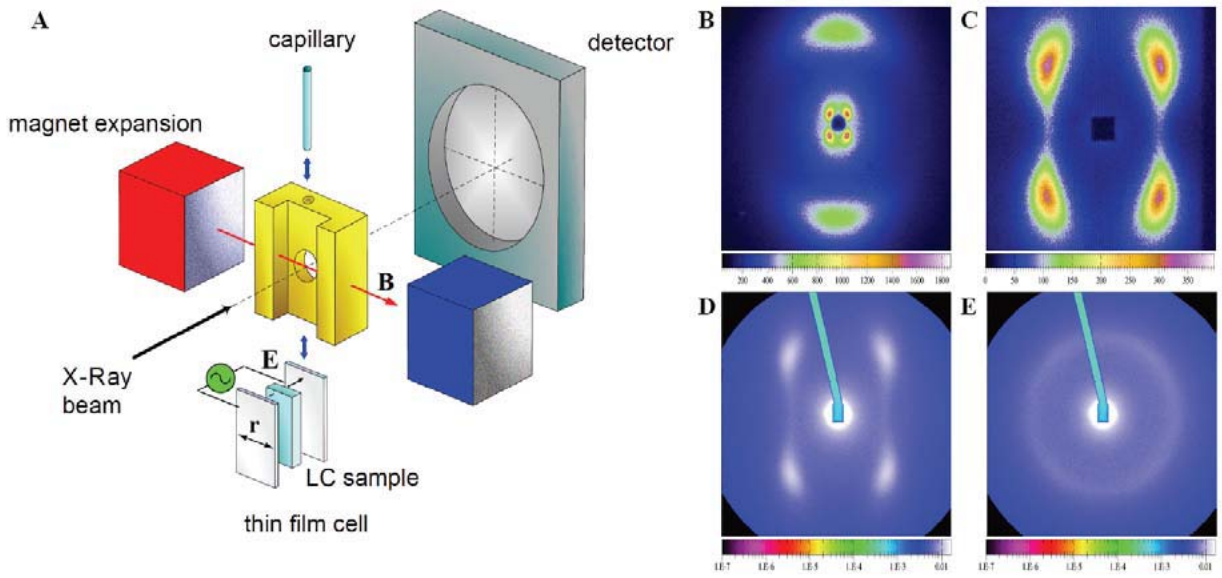

Figure 1.

(A) Schematic drawing of the experimental XRD setups (left) and synchrotron XRD patterns from the N phase at T=150 °C (right) with the thin film sample aligned by a magnetic (*B*) or electric (*E*) field applied either perpendicular to the beam direction or parallel to it.

The four images refer to (B) a capillary sample with *B*=0.5 T; (C) a close-up of the small angle region in image (B) showing the four symmetrically located diffuse spots as obtained at the BM26 beamline, ESRF; (D) a thin (20 μm) LC film sandwiched between SiO_x-covered glass plates aligning the director ***n*** in the LC cell parallel to ***r*** with *B*=0, *E*=0, and (E) the same cell with *B*=0 and *E*= 7.5 V/μm, 500 Hz, as obtained at the ID02 beamline, ESRF. In all patterns, the magnetic field lies along the horizontal axis

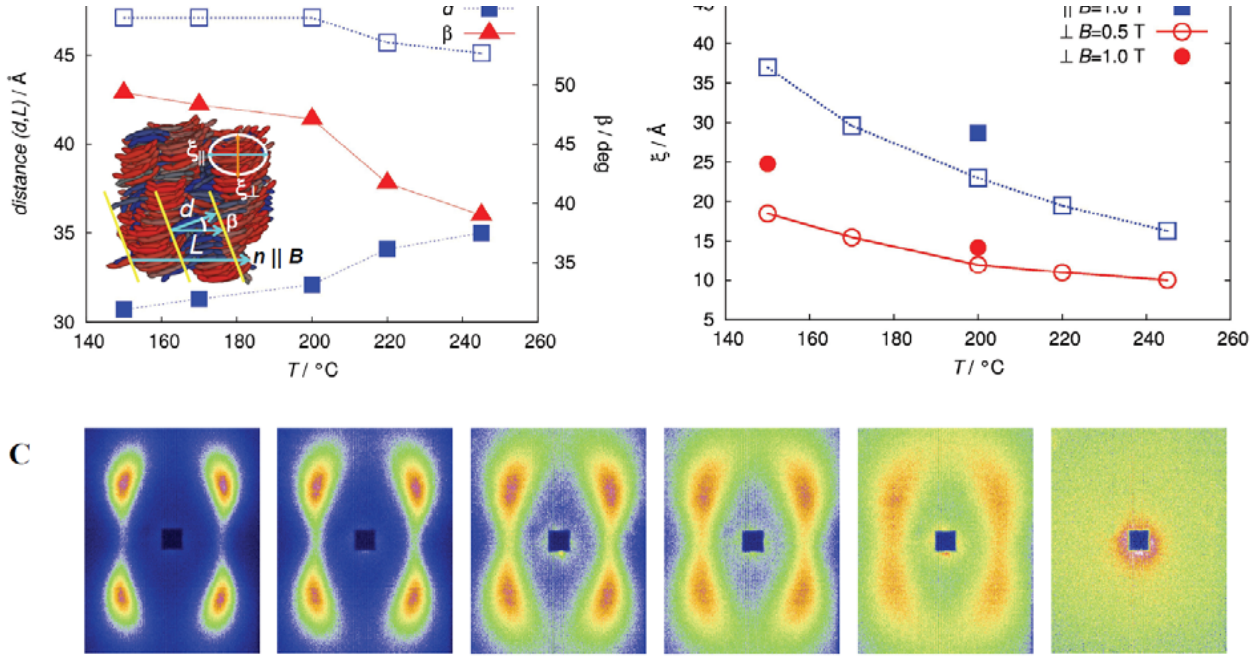

Figure 2.

(A) Structural parameters relevant to the cybotactic ordering as a function of temperature: *d* is the layer spacing, β is the tilt angle and $L=d/cos\beta$ is the apparent molecular length. In the inset, a simulation snapshot showing a few cybotactic groups with a representation of the above physical quantities.

(B) Spatial longitudinal ($\xi_{\parallel}$, blue squares) and transversal ($\xi_{\perp}$, red circles) correlation length, as a function of temperature, for two magnetic field values: 0.5 T (empty symbols) and 1.0 T (filled symbols). These quantities are calculated as $\xi_{\parallel,\perp}=2/\Delta q_{\parallel,\perp}$, where $\Delta q_{\parallel}$ and $\Delta q_{\perp}$ are the full width at half maximum (FWHM) of the Lorentzian lineshapes describing the profiles of the small-angle peaks in the reciprocal space, parallel and orthogonal to the magnetic field direction, respectively.

(C) Synchrotron SAXS patterns as a function of temperature. From the left to the right T=150, 170, 200, 220, 245 and 270 ˚C. Color coding (blue-green-yellow-purple red) for XRD intensities corresponds to the range 0-350, 0-300, 0-200, 0-180, 0-120 and 0-60 respectively. The magnetic field lies along the horizontal axis, as shown in Fig. 1A.

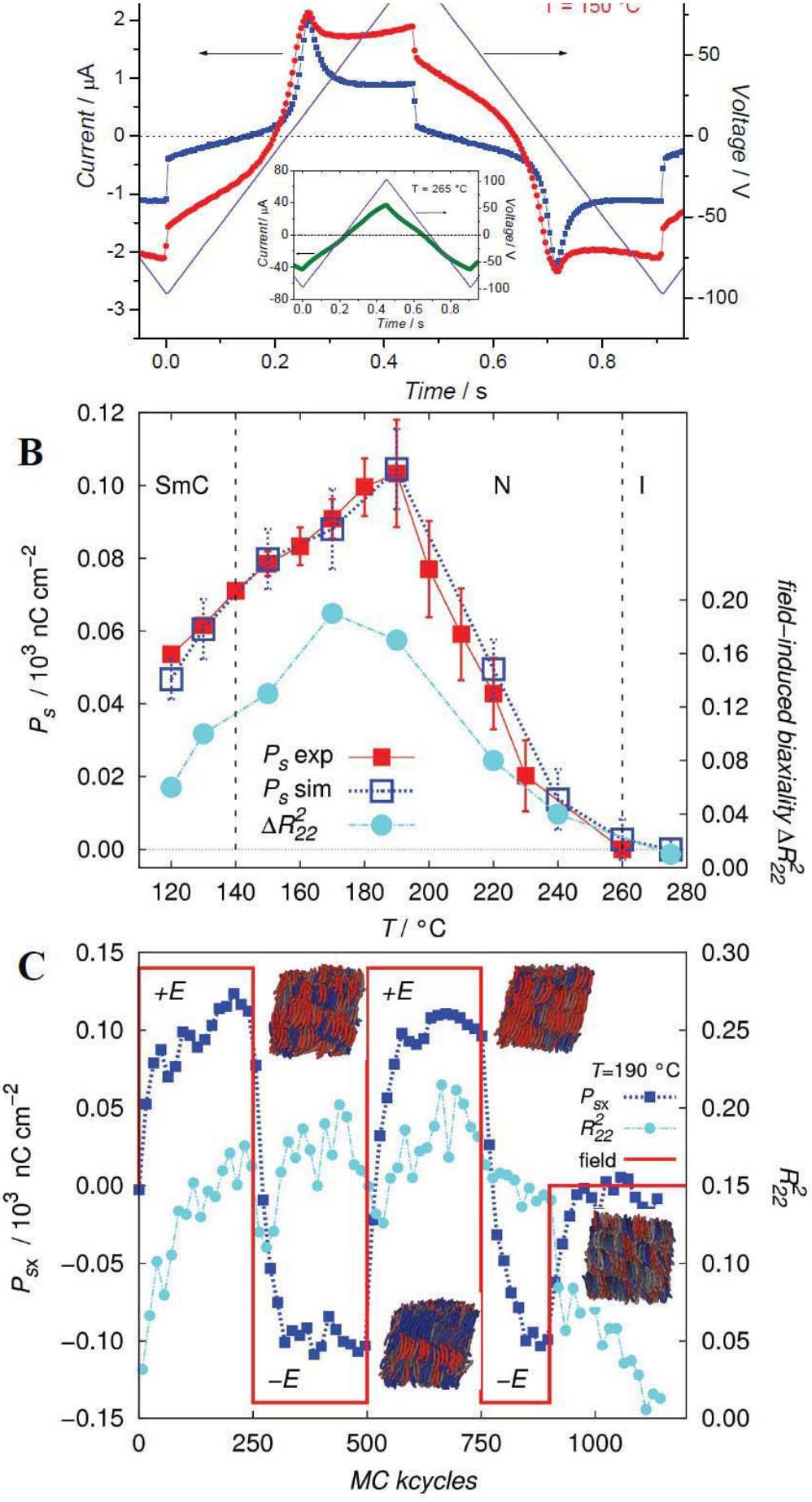
T = 150 °C
Current / μA
Voltage / V
Time / s
T = 265 °C
B
SmC
N
I
P_s / 10^3 nC cm^{-2}
field–induced biaxiality ΔR^2_{22}
P_s exp
P_s sim
ΔR^2_{22}
T / °C
C
+E
−E
T=190 °C
P_{sx}
R^2_{22}
field
P_{sx} / 10^3 nC cm^{-2}
R^2_{22}
MC kcycles

squares), 190 °C (N, red dots), 205 °C (I, in the inset, green), upon applying a triangular wave voltage (ν=1.1 Hz, V_{pp}=200 V, violet continuous line).

(B) Transverse polarization P_s response to an electric field E, as a function of the temperature, both from experiments (blue squares) and from MC simulations (red squares). The error bars are calculated from the statistical treatment of the repolarization current data over several periods of the input wave voltage. The difference between field-off and field-on biaxiality $\Delta R_{22}^2 = R_{22}^{2\,(\boldsymbol{E})} - R_{22}^{2\,(0)}$ (cyano circles) vs T is also reported.

(C) MC evolution, at T=190 °C, in the presence of an electric field $\boldsymbol{E}$ switching its sign every 250 kcycles and turned off after 900 kcycles. The instantaneous transversal (e.g. normal to the director) polarization P_{sx} (blue line, scale on the left) follows the field profile (cyan dashed line) with a delay of about 100 kcycles. The biaxiality order parameter R_{22}^2 (red line, scale on the right) grows almost irrespective of the field sign. The snapshots of the system after 250, 500, 750 and 1150 kcycles, show the alternation of prevalently red and blue polar domains depending on the sign of $\boldsymbol{E}$, and the eventual recovering of a non ferroelectric, uniaxial state.

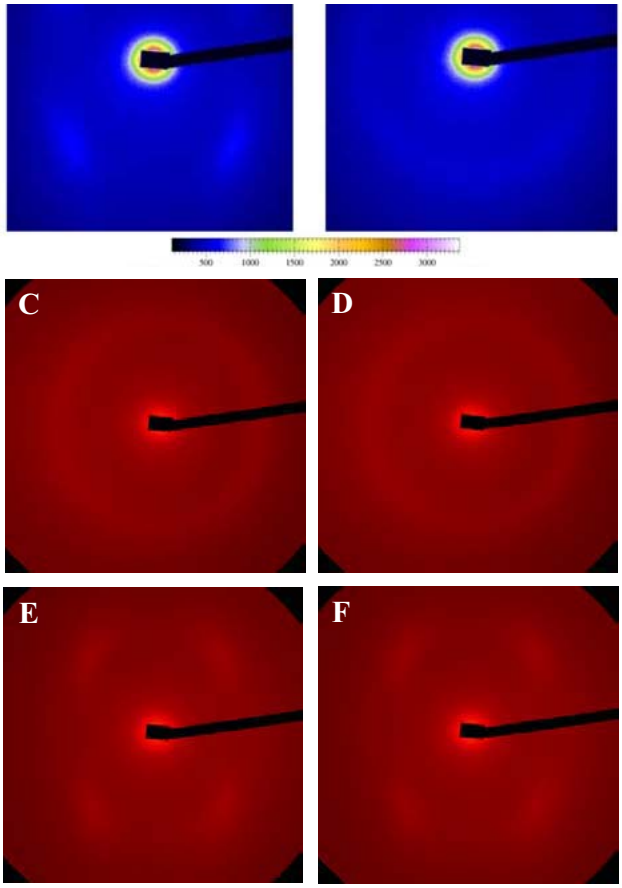

Figure 4. (A)-(B) Synchrotron XRD patterns from a thin (20 μm) sample film subjected to a low frequency square-wave voltage (ν=0.1 Hz, duty cycle=50%) above threshold: (A) before and (B) after the voltage step rise corresponding to the onset of the switching repolarization current peak. The film is sandwiched between SiO_x-coated glass plates aligning the director ***n*** in the LC cell parallel to ***r***. The temperature is T=150°C and the magnetic field is zero.
(C)-(F) Time resolved synchrotron XRD patterns of the same cell sample at T=150°C in the N phase: (C) dc E-field on (above threshold), and (D) 1 s, (E) 2 s, (F) 10 s and fter switching off the field. The acquisition time per frame is 0.5 s. No magnetic field is applied

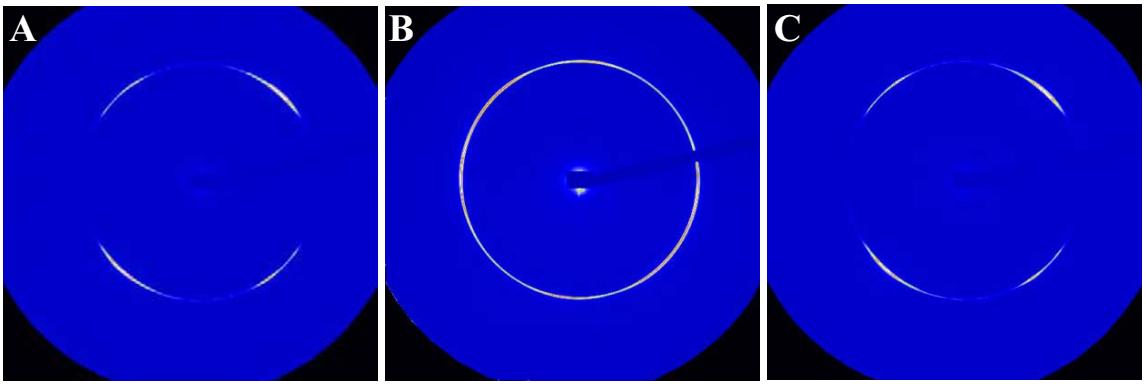

Figure 5. Small-angle XRD diffraction patterns of the planar thin-film cell sample at T=130°C in the SmC phase. (A) SmC uniaxially oriented by the planar surface anchoring parallel to the horizontal axis **r**, when **E**=0 and **B**=0. (B) SmC after application of an electric field **E** above threshold, normal to the glass plates (E=3.75 V/m, ν=1 Hz). The isotropic ring is consistent with a reorientation of the smectic domains with the polar axes parallel to the **E** and the normal to the smectic layers randomly distributed about **E**. (C) SmC under the same **E** field in the presence of a magnetic field B = 1.1 T parallel to **r**. A comparison with pattern A shows that no domain reorientation takes place when a magnetic field of enough strength is applied parallel to **r** to fix the long molecular axis.

core mesogens, allow a macroscopic ferroelectric switching due to the cooperative alignment of their cluster dipole. The nature of the mesophase and of the switching is demonstrated through X-ray and repolarization current measurements and coarse-grained computer simulations.

Keyword (Electro-optical Materials, Liquid Crystals)

O. Francescangeli*, V. Stanic, S. I. Torgova, A. Strigazzi, N. Scaramuzza, C. Ferrero, I. P. Dolbnya, T. M. Weiss, R. Berardi, L. Muccioli, S. Orlandi, C. Zannoni

Title: Ferroelectric response and induced biaxiality in the nematic phase of bent-core mesogens

ToC figure ((55 mm broad, 50 mm high, or 110 mm broad, 20 mm high))

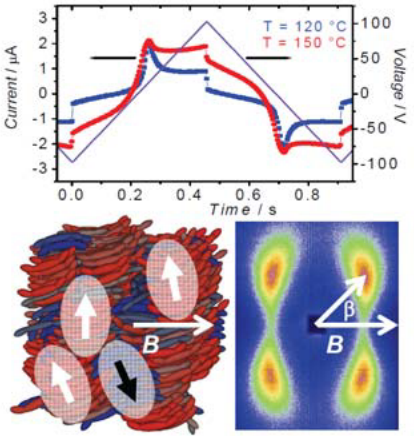

The electro-optic analysis was performed in combination with the repolarization current measurements, by subjecting the planar LC cell (10 μm) to a triangular wave voltage and observing the optical texture between crossed polarizers.

In a first set of measurements the polarizing direction of the microscope was set parallel to ***r***. In these conditions the image is completely dark at zero field. Videoclip 1 shows the data recorded at T=145 °C over a few periods of the input wave voltage (ν=0.5 Hz). The periodic alternation of dark and brighter images with frequency twice that of the input wave voltage is due to the rotation of the director out of the incident plane consequent to the field-induced reorientation of the polar cybotactic domains. The relatively poor intensity contrast between *dark* and *bright* images is consistent with the reorientation of the cybotactic groups with their dipolar axes parallel to the field and the long molecular axes essentially isotropic distributed around the field direction, in agreement with the XRD data.

In a following set of measurements the polarizing direction of the microscope was set to 45° with respect to the direction ***r*** of uniform planar orientation of the director. In these conditions the images are bright at zero field. Videoclips 2-3 show the data recorded in the nematic phase at T=170 °C and T=200 °C, respectively, over a few periods of the input wave voltage (ν=0.5 Hz, V_{pp}= 60 V). The regular alternation of bright and dark images corresponds to a periodic modulation with frequency twice that of the input wave voltage, which is consistent with the reversal of the polarization direction every half period of the input voltage. The combination of these results with those of repolarization current measurements provide clear evidence of the existence of a switchable macroscopic polar domain. A very similar electro-optic response is observed in SmC phase, as shown by the videoclip 4 recorded at T=130 °C (ν=0.2 Hz, V_{pp}= 50 V).

Video1.wmv

Videoclip 1. Electro-optic response of the BM 9BPO in the nematic phase at T=145 °C (v=0.5 Hz). The polarizer is parallel to ***r***.

Video2.wmv

Videoclip 2. Electro-optic response of the BM 9BPO in the nematic phase at T=170 °C (v=0.5 Hz, V_{pp}=60 V). The polarizer is at 45° to ***r***.

Video3.wmv

Videoclip 3. Electro-optic response of the BM 9BPO in the nematic phase at T=200 °C (v=0.5 Hz, V_{pp}=60 V). The polarizer is at 45° to ***r***.

Video4.wmv

Videoclip 4. Electro-optic response of the BM 9BPO in the smectic C phase at T=130 °C (v=0.2 Hz, V_{pp}=50 V). The polarizer is at 45° to ***r***.

These Supporting Information Videos are also available at the following link:
http://www2.fci.unibo.it/~luca/webdoc/Videos.rar

A peculiar advantage of atomistic computer simulations is the possibility to explore all possible molecular conformations accessible at a given temperature and in a given phase. This is particularly interesting for a flexible molecule such as 9PBO, for which the concept of molecular length cannot be uniquely defined. Molecular dynamics results actually allow extending this concept to the one of distribution of the molecular length, which is expected to be more appropriate for a partly flexible molecule. Here, like in [43, 44], we consider as molecular dimension indicator the sides of the minimal rectangular box containing the molecule rotated in its inertial frame, and we label "molecular length" L_{MD} the longest side. From Supporting Info Figure 2, where we show the distribution of this quantity in two different phases, isotropic and nematic, it is apparent that for 9BPO important changes in the molecular shape can occur in the temperature range studied. Another important finding is that at both temperatures this distribution is very broad, revealing a number of possible conformations with very similar probability. Finally, it is worth noting that the maximum of the distribution in the nematic phase, at 45-47 Å, is in very good agreement with the apparent molecular length L measured by X-ray at similar temperatures, reported in Figure 2 of the manuscript.

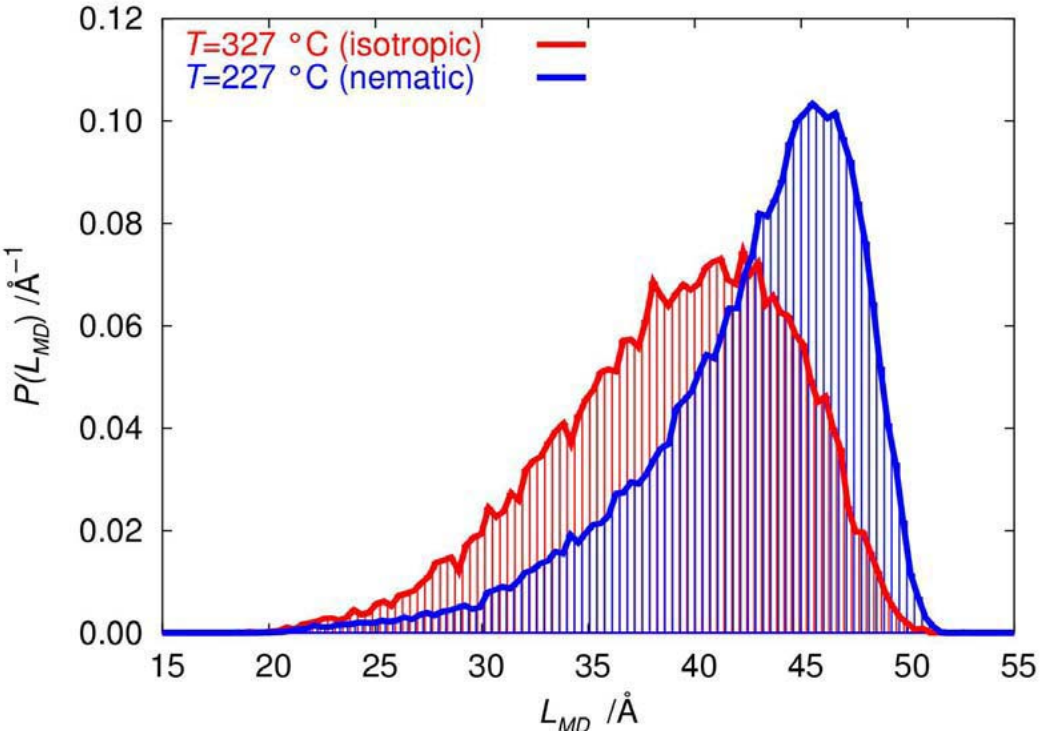

Figure 2. Distribution of the molecular length of 9BPO, obtained from united atom atomistic simulations of the isotropic phase (in red, 327 ˚C, $R_{00}^2 \approx 0.13$), and of the nematic phase (in blue, 227 ˚C, $R_{00}^2 \approx 0.70$).

ordering and biaxiality, the equilibrium MC configurations were collected and analysed to calculate various orientational order parameters [49]. In particular, structural assignment requires knowledge not only of the order of a molecule with respect to the laboratory frame, but also of the arrangement of one molecule with respect to another at a certain distance, as obtained via various pair distribution functions computed as discrete histogram from the simulated configurations. In particular the second rank orientational pair correlation $S_{22}^{220}(r)$ (see [55]) is useful in assessing the local biaxiality and its correlation length.

As a further information on the polar correlations between molecular axes we have computed the average scalar product $P_{1x}(r) =< \delta(r - r_{ij})\boldsymbol{x}_{.i} \cdot \boldsymbol{x}_j >$ between the transverse axis $\boldsymbol{x}_i$ of a molecule i chosen as origin and that of any molecule j found at a distance r.

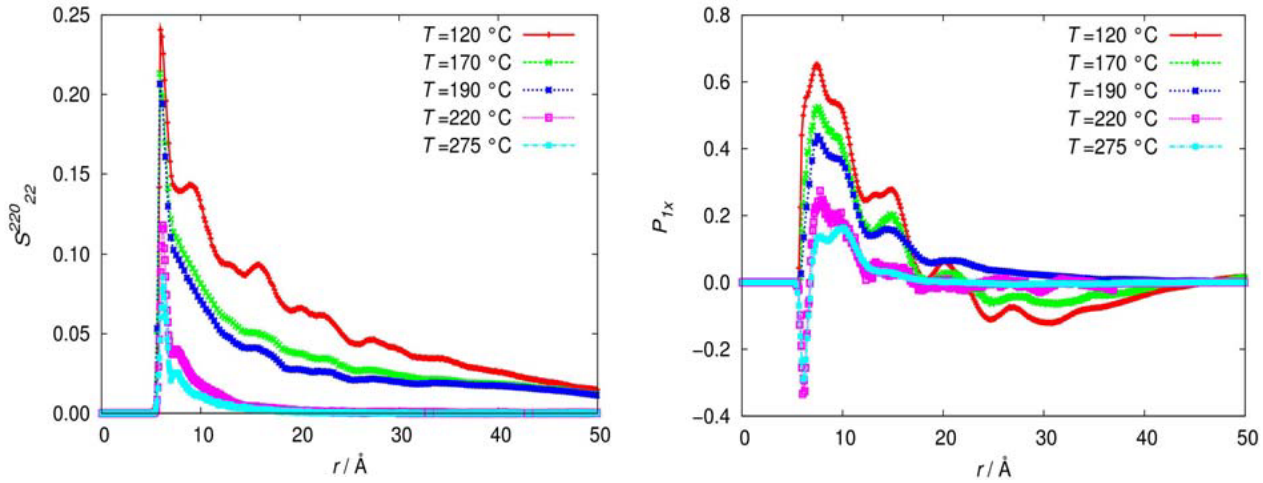

Figure 3. (A) Second rank orientational pair correlation $S_{22}^{220}(r)$ and (B) $P_{1x} =< \delta(r - r_{ij})\boldsymbol{x}_{.i} \cdot \boldsymbol{x}_j >$ in the smectic C (T=120 ˚C), nematic (T=170,190,220 ˚C) and isotropic phase (T=275 ˚C).

The analysis of these correlation functions (Figure 3) evidences a long range decay behaviour of $S_{22}^{220}(r)$ in smectic and nematic phases, up to 190˚C (Figure 3A), while the polar pair correlation $P_{1x}(r)$ shows an average overall persistence of 20-25 Å, as shown by Figure 3B, then decays to zero. This indicates a polar arrangement of dipoles on a cybotactic group, also evident from the local red and blue domains in the snapshots (Figure 4). It is also

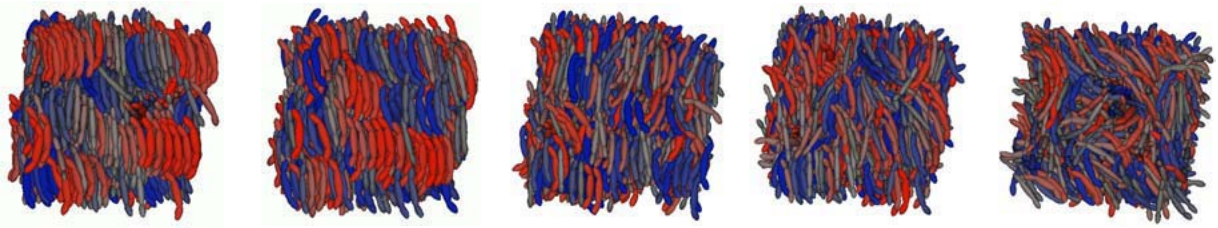

Figure 4. Simulation snapshots at different temperatures, color-coded according to the polar orientation of the ***x*** molecular axis with respect to the nematic director ***n***, ranging from red (***n***.***x***=+1) to blue (***n***.***x***=-1).